5

MoSSe and WSSe monolayers with and without defects for gas sensing applications

5.1 Introduction

The most efficient industrialized gas sensor materials are metal oxide semiconductors like ZnO and SnO_2 (Jian Zhang, Qin, Zeng, & Xie, 2017). The advantages of these materials are their high sensitivity and cost-effectiveness. However, disadvantages are operating temperature, large power consumption, and selectivity (C. Wang, Yin, Zhang, Xiang, & Gao, 2010). The carbon nanotube-based materials can surpass the problem of the metal oxide semiconductors. But the recovery time and complex handling are the limiting factors for such materials towards their industrialization. Graphene has shown credentials like ultrahigh sensitivity, selectivity, and low power requirement (Camilli & Passacantando, 2018; C. Wang et al., 2010). Moreover, the small electrical noise can induce a very high signal to noise ratio. The working principle of 2D materials based gas sensor is based on the charge transfer amongst the adsorbate and host (Wang, Yun, Yeow, 2009). Other important 2D materials are TMDs, BN, Mxenes, and phosphorene, which are used extensively for gas adsorption (Zaporotskova, Boroznina, Parkhomenko, & Kozhitov, 2016). The semiconductor behavior of the TMDs leads to changes in electrical properties with external perturbations; that's why TMDs may show excellent sensing characteristics.

Janus MoSSe and WSSe monolayers are investigated as a host material for gas sensing of hazardous gases. Since the conventional TMDs based monolayers are defect prone; that's why the study of possible defects in the MoSSe and WSSe monolayers also studied. The sensing behavior of the gases is studied in terms of the adsorption energy, charge transfer, electronic, and magnetic properties. The electronic and magnetic properties of defect included MoSSe, and WSSe monolayers are studied and also explored for gas sensing applications. These defects may help to create the active site for adsorption of the gas molecules and help to improve the sensitivity and selectivity.

5.2 Computational Details

The ground-state properties of Janus MoSSe and WSSe monolayers are studied using the QE package (Giannozzi et al., 2009b; Kohn & Sham, 1965b). A 4x4 supercell and 15 Å void along c-axis is considered for investigating the effect of the defect and gas sensing properties. The GGA-PBE is used as the exchange-correlation functional in these calculation (Tasker, 1996). Ultrasoft pseudopotentials are used to define the core cell potential of atom. The wave function cutoff energy is fixed around 50 Ry. The BZ of supercell is sampled according to the Monkhorst-Pack (Pack & Monkhorst, 1977) scheme using 6x6x1 K-points for optimization and 12x12x1 K-points for electronic and gas sensing properties. The SCF energy cutoff is set at $1x10^{-8}$ Ry. Force and energy cutoff between the two consecutive SCF cycle set at $1x10^{-3}$ and $1x10^{-4}$, respectively. DFT-D2 method is used to evaluate the vdW interaction (Grimme, 2006). The vacancy and antisite defects in a supercell are introduced by removing and replacing the atoms, respectively. The stability of defects is confirmed through the formation energy:

$$E_f^{vac} = E_{tot}^{def} - E_{tot}^{pris} + E_{removed}^{X}$$
$$E_f^{anti} = E_{tot}^{def} - E_{tot}^{pris} + E_{removed}^{X} - E_{added}^{Y}$$

Where, E_f^{vac} andE_f^{anti} are the formation energy of vacancy and antisite defect. E_{tot}^{def}, E_{tot}^{pris}, $E_{removed}^{X}$ and E_{added}^{Y} are the total energy of the defect included monolayer, pristine monolayer, removed atom and added atom, respectively.

To study the gas sensing properties on pristine and defect included monolayers, we took H_2S, NH_3, NO_2, and NO gas molecules. The adsorption of gas molecules is evaluated with different orientations on the pristine, and defect included monolayers. The adsorption energy is used to estimate the stability of adsorbed gas molecules.

$$E_{ad} = E_{monolayer+gas} - (E_{monolayer} + E_{gas})$$

Where $E_{monolayer+gas}$, $E_{monolayer}$ and $E_{gas}$are the total energy of gas molecule adsorbed monolayer, without gas adsorbed monolayer and gas molecules.

The gas molecules are adsorbed with different orientations on the host from both sites, as shown in Figure 5.1. Adsorption energy with the negative value is indicating the favorable condition gas sensing (Basharnavaz, Habibi-Yangjeh, & Mousavi, 2018). The adsorption of the gas molecule is also investigated through the electronic properties. The sensing response is attributed to the change in the electrical conductivity due to the adsorption of gas molecules, causing the charge sharing between the adsorbate and host. The charge transfer is investigated from the Bader charge analysis (Henkelman, Arnaldsson, & Jónsson, 2006). Recovery time is also an important parameter for gas sensor, which depends on the adsorption energy (Roondhe, Patel, & Jha, 2019). It should be as small as possible so that gas molecules can easily desorb from the host surface.

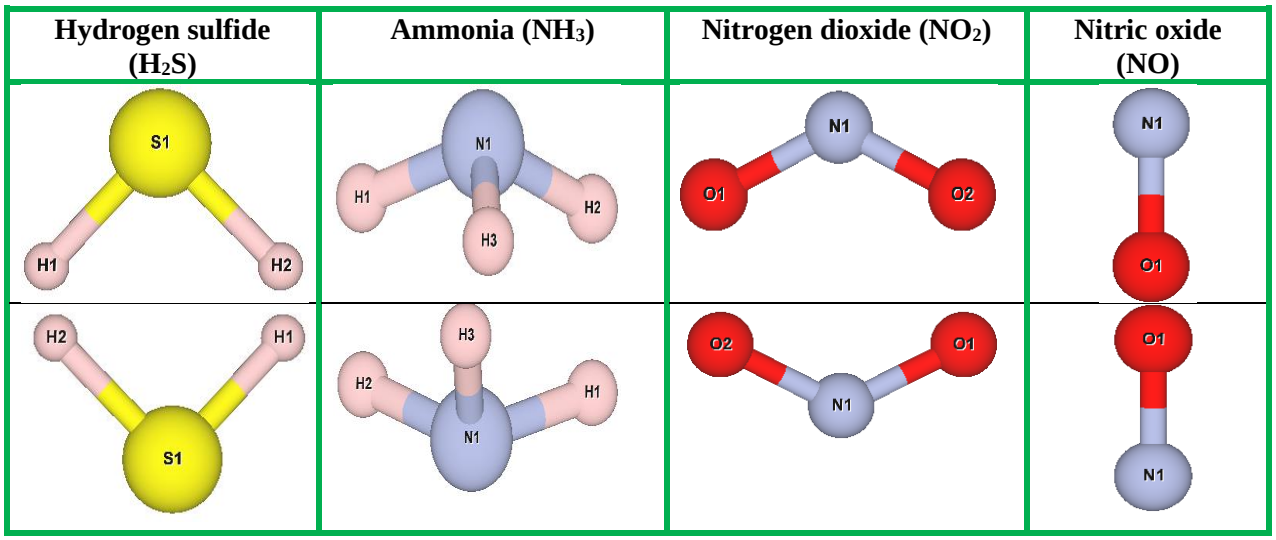

Figure 5.1 Schematic representation of initial geometry of H_2S, NH_3, NO_2 and NO molecule

5.3 Results and Discussion

5.3.1 Electronic properties of antisite defect including WSSe monolayers

The structural and electronic properties of the WSSe monolayer are discussed in chapter 4. Various vacancy and antisite defects in WSSe monolayer are considered and studied the detailed structural, electronic, and magnetic properties. The results are reported by Chaurasiya et al.(Chaurasiya & Dixit, 2020). Here, we considered the two antisite defect sulfur replaced selenium (WSSe@Sse) and selenium replaced by sulfur (WSSe@Ses) monolayer in the supercell, which is equivalent to 2.08% antisite defect density. The formation energy for WSSe@Ses and

WSSe@Sse defects are -0.76eV and 0.03 eV, which is very small compared to other point defects. The bond length near the defect point is not changing significantly due to a little change in the ionic radii of sulfur and selenium atoms. The band structure is shown in Figure 5.2 along with TDOS for WSSe@Sse and WSSe@Ses monolayers. WSSe@Ses and WSSe@Sse monolayers show the direct bandgap 1.61 eV and 1.57eV at the K point of BZ. The electronic properties of considered antisite defects show the small change in bandgap due to similar electronic configuration of sulfur and selenium atoms. The symmetric contribution of spin up and spin down states ensure the non-magnetic semiconducting behavior. The PDOS of WSSe@Sse and WSSe@Ses monolayers are shown in Figure 5.2. The valence band and conduction band edges are mainly dominated by the W-d orbital, and deep region (below -1.5 eV) of valence band is contributed by the S/Se-p orbitals.

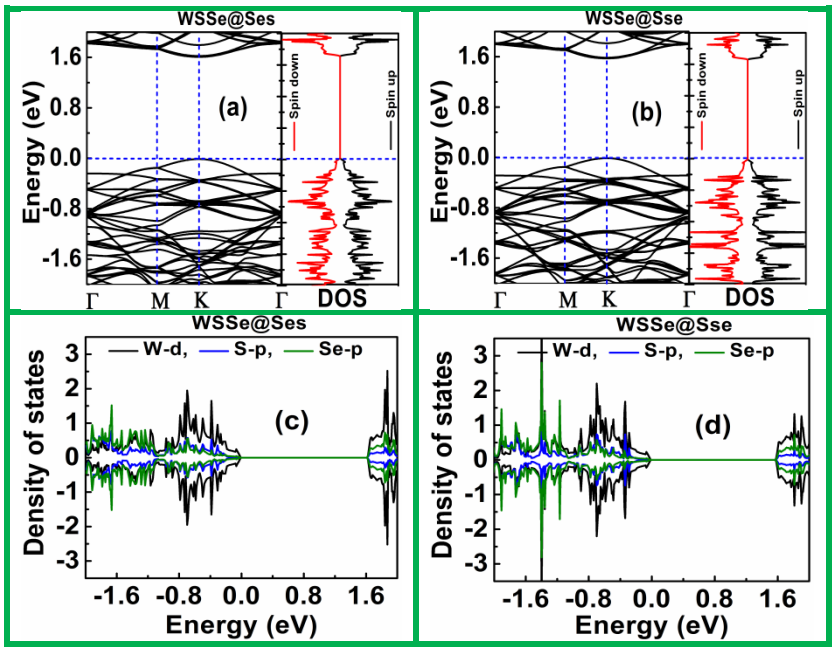

Figure 5.2 (a) and (b) are the band structure; (c) and (d) are PDOS of WSSe@Ses and WSSe@Sse monolayer, respectively.

5.3.2 Adsorption of toxic gas molecules on pristine WSSe monolayer

In this part, four gas molecules, H_2S, NH_3, NO_2, and NO are considered as the adsorbate. H_2S molecule is allowed to adsorb from hydrogen and sulfur site towards the host. Figure 5.1 shows the orientation of H_2S molecule for adsorption. The selenium surface and sulfur surface of WSSe monolayer are represented as WSSe_Se and WSSe_S, which are considered as hosts for adsorption. The relaxed geometries of WSSe_Se/H_2S, WSSe_Se/H_2S1, WSSe_S/H_2S, and WSSe_S/H_2S1 are illustrated in Figure 5.3(a-d) along with the Bader charge analysis and adsorption height. The adsorption lengths are differing in the range of 2.49 to 3.37 Å, which is more than the summation of ionic radii of the top surface of host and lower surface of adsorbate and thus, confirming the vdW interactions. The minimum adsorption distance, 2.49Å is found for WSSe_Se/H_2S arrangements because of the different nature of the charge of H (H_2S) and Se surface. However, the adsorption length is found 3.37 Å for WSSe_S/H_2S1 due to the repelling of similar charge of S (H_2S) atom and S surface. The adsorption height is relatively less when H_2S adsorb from the hydrogen site over the sulfur site due to Columbic interaction in two different atomic charges. Bader charge showed the more charge transfer 0.011e and 0.008e for WSS_Se/H_2S and WSSe_S/H_2S, respectively compare to WSS_Se/H_2S1 and WSSe_S(H_2S1). All the considered arrangements showed the charge depletion from the WSSe monolayer, which confirm the acceptor nature of H_2S. The CDD plots, Figure 5.4(a-d) validate the Bader charge analysis and adsorption length. The SPDOS of spin up and spin down states for all arrangements are depicted

in Figure 5.5(a&b) and compared with the pristine monolayer. The adsorption of H_2S molecule doesn't show additional states in the forbidden region, which confirms the strong overlapping of electronic states of WSSe and H_2S orbital. The symmetry in the spin up and spin down states confirm the non-magnetic behavior after the adsorption of H_2S molecule.

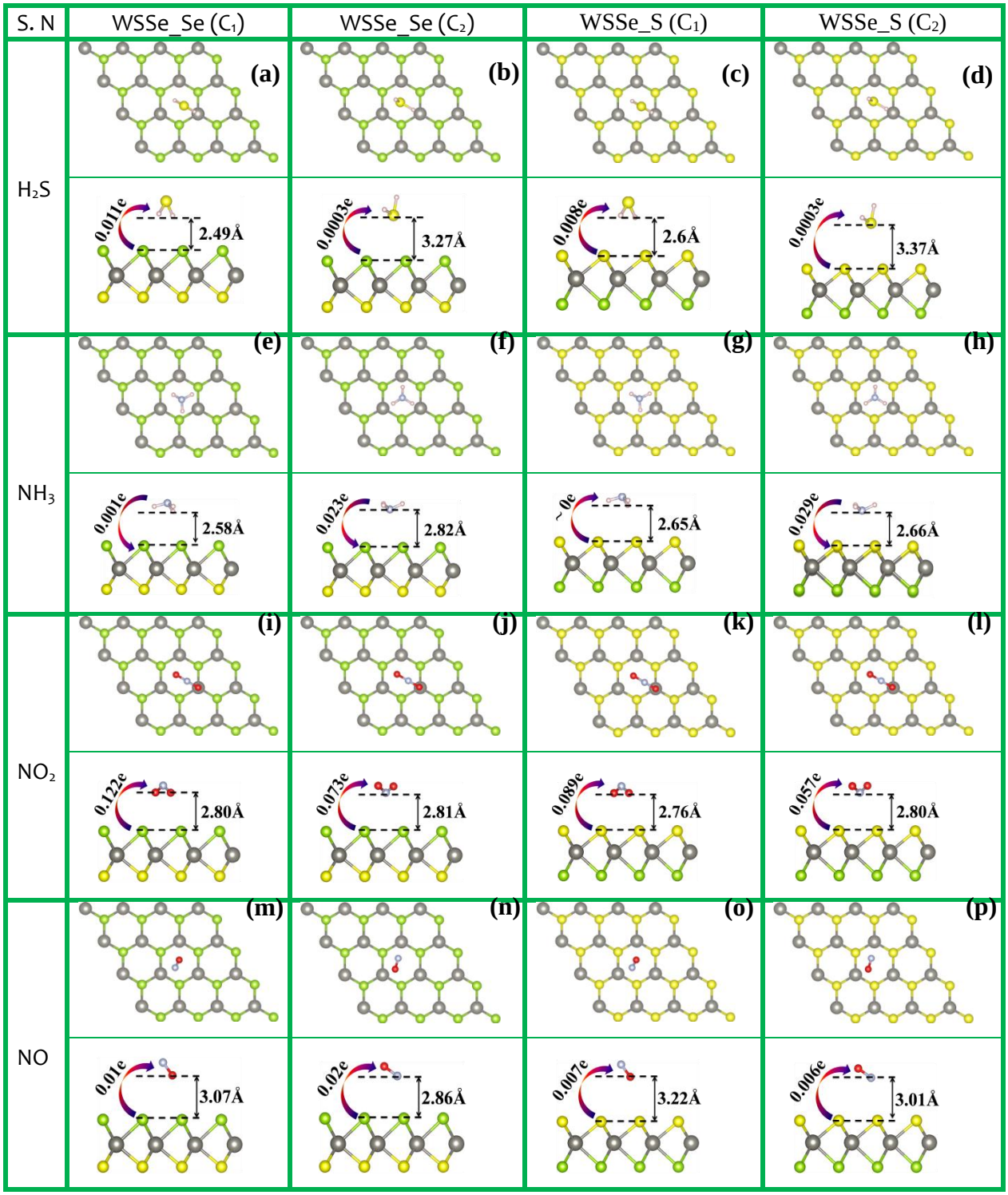

Figure 5.3 Optimized structures of H_2S (a–d), NH_3 (e–h), NO_2 (i–l) and NO (m–p) molecules adsorbed on the selenium and sulfur surfaces of the WSSe monolayer. (The WSSe_Se(C1) arrangements ensure the molecule adsorb from H in H_2S, H in NH_3, O in NO_2 and O in NO site. WSSe_Se(C2) arrangements ensure the molecule adsorb from S in H_2S, N in NH_3, N in NO_2 and N in NO site. WSSe_S(C1) arrangements ensure the molecule adsorb from H in H_2S, H in NH_3, O in NO_2, and O in NO site. WSSe_S(C2) arrangements ensure the molecule adsorb from S in H_2S, N in NH_3, N in NO_2, and N in NO site.)

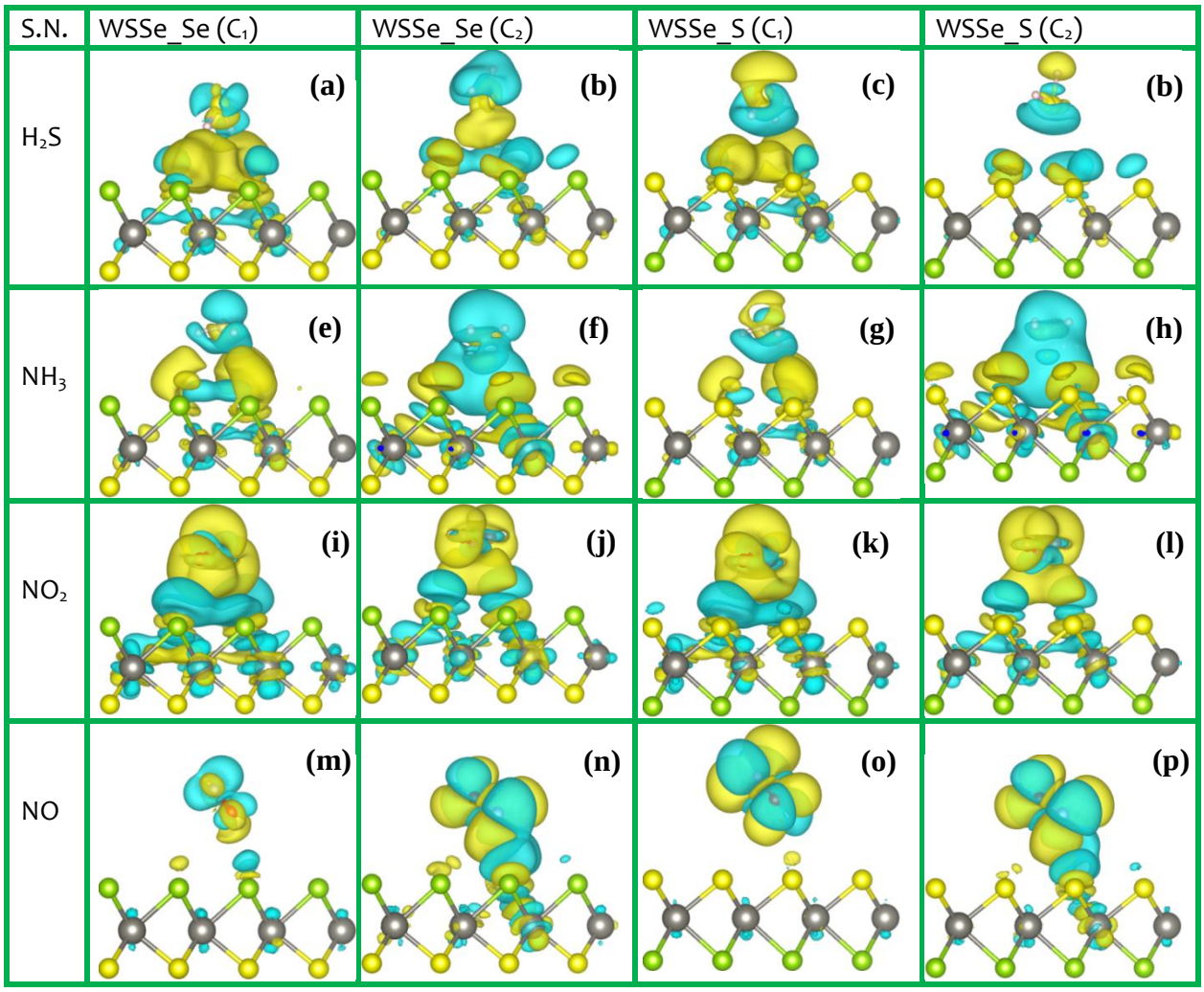

Figure 5.4 (a-d) H_2S, (e-h) NH_3, (i-l) NO_2 and (m-p) NO charge density difference. (Isosurface value 10^{-4} e/Å^3, yellow color corresponds to charge accumulation, and blue color corresponds to charge depletion)

The NH_3 molecule is also allowed to adsorb from the hydrogen and nitrogen site on the WSS_Se, and WSSe_S surfaces and arrangements are represented as WSSe_Se/NH_3, WSSe_Se/$NH_3$1, WSSe_S/NH_3 and WSSe_S/$NH_3$1, Figure 5.3(e-h) along with the respective charge transfer, and adsorption lengths. The adsorption heights for these arrangements vary in the range of 2.58 to 2.82Å. The minimum adsorption height is found for WSSe_Se/NH_3 arrangements due to Columbic interaction and the maximum adsorption height for WSSe_Se/$NH_3$1 due to the repulsion between similar types of charge. The above-studied adsorption height is suggesting the physisorption between the adsorbate and host. The Bader charge analysis shows the charge transfer in the range of 0.023e to 0.029e charge from adsorbate to host because the Fermi level of the host may lie below the HOMO of adsorbate. The CDD plots for arrangements based on NH_3 adsorption endorse the Bader charge analysis. The adsorption height for the NH_3 molecule is comparatively lower than the H_2S molecule due to superposition of host and adsorbate electric dipoles. The introduction of the electric field is responsible for improving the gas sensing properties, as observed in case of MoS_2 monolayer (C. Jin et al., 2019). The SPDOS for all the considered arrangements are illustrated in Figure 5.5(c&d), showing the strong orbital overlapping of adsorbate and host.

The NO_2 molecule is also investigated as an adsorbate on WSSe_Se and WSSe_S monolayer, which is allowed to adsorb from the N and O atomic sites. The various arrangements for NO_2 adsorption are WSSe_Se/NO_2, WSSe_Se/$NO_2$1, WSSe_S/NO_2 and WSSe_Se/$NO_2$1, shown in

Figure 5.3(i-l). The adsorption height varies from 2.76 to 2.81Å for different arrangements. The Bader charge analysis shows the 0.057e to 0.122e charge transfer for various arrangements. The CDD plots, shown in Figure 5.4(i-l), validate the Bader charge analysis. The charge is transferring from host to adsorbate; ensure the acceptor nature of adsorbate because the LUMO of adsorbate may lie below the Fermi level of the host. Figure 5.5(e&f) shows the SPDOS for all the arrangements and shows the flat bands in the VB and CB and asymmetry in spin up and spin down, induce of $1\mu_B$ magnetic moment due to NO_2 adsorption.

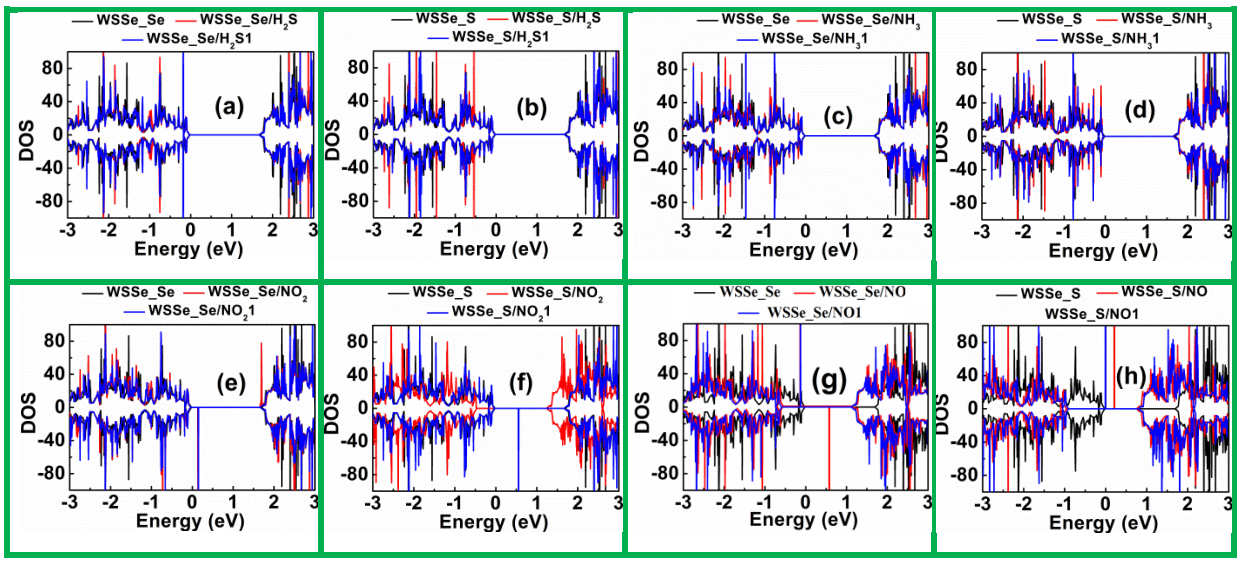

Figure 5.5 Comparison of SPDOS of pristine monolayer and molecule adsorbed monolayer (a&b) H_2S, (c&d) NH_3, (e&f) NO_2 and (g-h) NO.

NO molecule is also evaluated as an adsorbate on WSSe monolayer. The NO molecule is explored to adsorb from the N, and O atom sites and possible arrangements are WSSe_Se/NO, WSSe_Se/NO1, WSSe_S/NO and WSSe_S/NO1 are depicted in Figure 5.3(m-p). The Bader charge analysis shows 0.006e to 0.02e charge transfer from host to adsorbate, confirming the charge accumulation nature of NO molecule. The adsorption height is varied from 2.86 to 3.22Å, respectively, for different arrangements. The CDD plots validate the Bader charge analysis. The adsorption height and CDD suggests the physisorption between the adsorbate and host. The SPDOS for different arrangements are shown in Figure 5.5(g&h), showing the additional states due to NO adsorption and asymmetry in spin up and spin down states endorse the onset of $1\mu_B$ magnetic moment.

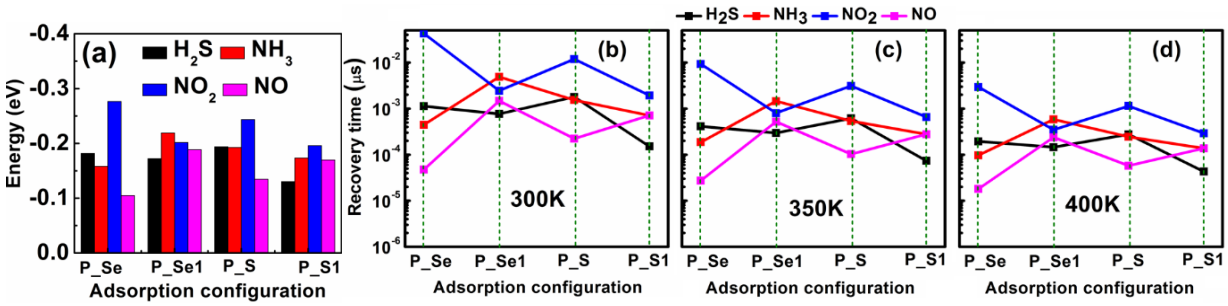

Figure 5.6 (a) Adsorption energy and (b-d) temperature dependent recovery times of molecules adsorb on selenium and sulfur surface of monolayer.

We have computed the adsorption energy for different arrangements and shown in Figure 5.6(a). The temperature-dependent recovery time is reported in Figure 5.6(b-d). The recovery time strongly depends on the adsorption energy. The adsorption energy and recovery time should be

optimum so that the gas sensor can sense i.e. adsorb and desorb easily. The adsorption energy of H_2S molecule is varied in the range of 0.13 eV to 0.19 eV, and the corresponding recovery time is $1.5x10^{-4}$μs and $1.5x10^{-3}$μs, respectively. When the H_2S molecule is adsorbed from the hydrogen site at the selenium surface, the maximum adsorption energy is noticed. The Janus WSSe showed a higher sensitivity compared to other monolayers, reported in table 5.1. The adsorption energies are - 0.16 eV, - 0.22 eV, - 0.19 eV, and - 0.17 eV for WSSe_Se/NH_3, WSSe_Se/$NH_3$1, WSSe_S/NH_3 and WSSe_S/$NH_3$1 arrangements, respectively. The recovery time for adsorption of NH_3 molecule at room temperature is plotted in Figure 5.6(b). The adsorption energy of NH_3 on WSSe monolayer higher than the other TMDs monolayer reported in table 5.1. Figure 5.6(a) shows the adsorption energy of NO_2 molecule for different arrangements, maximum adsorption energy - 0.28 eV is found for WSSe_Se/NO_2 arrangements, and corresponding recovery time is $4.3x10^{-2}$μs. The adsorption energy for the NO molecule is presented in Figure 5.6(a). The adsorption energies are – 0.10 eV, - 0.19 eV, - 0.14 eV and 0.17 eV for WSSe_Se/NO, WSSe_Se/NO1, WSSe_S/NO, and WSSe_S/NO1, respectively. The adsorption energies of all the considered molecules evaluated on both the surfaces of WSSe monolayer and compared with the other reported TMDs monolayers, reported in table 5.1. The selenium surface shows the more sensitivity compared to the sulfur surface because of high electrostatic potentials correspond to the selenium surface.

Table 5.1 Comparison of adsorption energy and Bader charge analysis of widely used monolayers

Adsorbent	Properties	H_2S	NH_3	NO_2	NO	Theory	References
WSSe monolayer	E_{ads} (eV)	- 0.193	- 0.220	- 0.276	- 0.189	GGA & DFT-D2	This work
	Q (e)	0.008	- 0.023	0.122	0.020		
MoSSe monolayer	E_{ads} (eV)	NA	- 0.200	- 0.242	- 0.150	GGA & DFT-D3	(C. Jin et al., 2019)
	Q (e)	NA	-0.031	0.107	0.038		
WS_2 monolayer	E_{ads} (eV)	NA	- 0.180	- 0.206	- 0.132	GGA & DFT-D2	(Babar, Vovusha, Schwingenschlögl, 2019)
	Q (e)	NA	NA	NA	NA		
WSe_2 monolayer	E_{ads} (eV)	NA	- 0.042	- 0.067	- 0.025	GGA	(T. Wang et al., 2016)
	Q (e)	NA	- 0.017	0.116	0.034		
MoS_2 monolayer	E_{ads} (eV)	Na	- 0.160	- 0.169	- 0.114	GGA & DFT-D2	(Babar et al., 2019)
	Q (e)	NA	NA	NA	NA		
MoS_2 monolayer	E_{ads} (eV)	NA	- 0.195	- 0.208	- 0.138	GGA & DFT-D3	(C. Jin et al., 2019)
	Q (e)	NA	- 0.036	0.055	- 0.005		
$MoSe_2$ monolayer	E_{ads} (eV)	NA	- 0.195	- 0.252	- 0.140	GGA & DFT-D3	(C. Jin et al., 2019)
	Q (e)	NA	- 0.025	0.117	0.017		
MoS_2/WS_2heterobilayer, MoS_2 side	E_{ads} (eV)	NA	- 0.166	- 0.116	- 0.177	GGA & DFT-D2	(Babar et al., 2019)
	Q (e)	NA	NA	NA	NA		
MoS_2/WS_2heterobilayer, WS_2 side	E_{ads} (eV)	NA	- 0.186	- 0.213	- 0.135	GGA & DFT-D2	(Babar et al., 2019)
	Q (e)	NA	NA	NA	NA		
$HfSe_2$ monolayer	E_{ads} (eV)	- 0.86	- 0.149	- 0.171	- 0.193	GGA & DFT-D2	(Yang et al., 2019)
	Q (e)	- 0.01	0.002	0.053	- 0.054		
Graphene	E_{ads} (eV)	NA	- 0.031	- 0.067	- 0.029	GGA	(Leenaerts, Partoens, & Peeters, 2008)
	Q (e)	NA	0.027	- 0.102	0.017		
h-BN monolayer	E_{ads} (eV)	NA	- 0.10	- 0.125	- 0.117	LDA	(Pashangpour, 2011)
	Q (e)	NA	0.017	0.039	0.005		

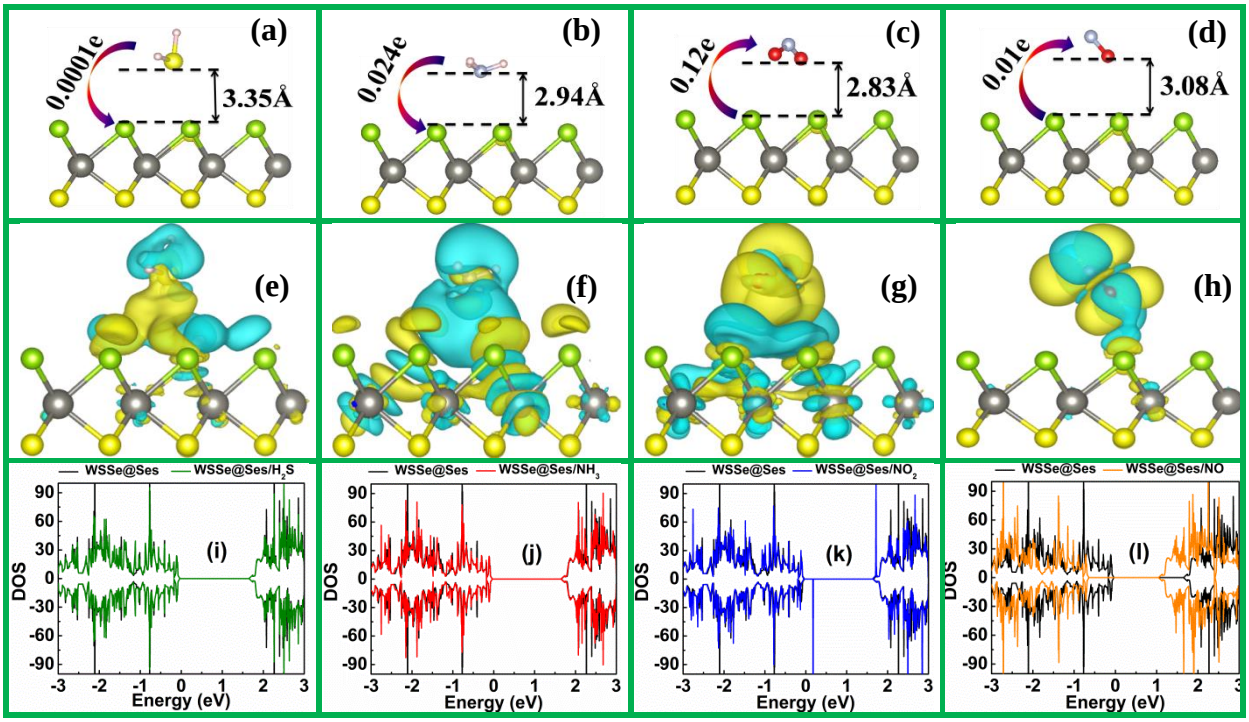

Figure 5.7 (a-d) Optimized geometries, (e-h) charge density difference and (i-l) SPDOS of gas molecules adsorb on WSSe@Ses monolayer. ((Isosurface value 10^{-4} e/Å^3, the yellow color corresponds to charge accumulation, and blue color corresponds to charge depletion)

5.3.3 Adsorption of toxic gas molecules on antisite defect including WSSe monolayers

The adsorption of the H_2S molecule is examined on the WSSe@Ses monolayer. The optimized geometry shows the 3.35 Å adsorption height and 0.0001e charge transfer from host to adsorbate, represented in Figure 5.7(a). The CDD plot also shows the charge accumulation near the adsorbate. Adsorption energy and CDD plot signify the vdW interaction between the adsorbate and host. The bond length of the H_2S molecule enlarges by 0.002Å after adsorption. The computed adsorption energy found - 0.176 eV and corresponding recovery time is $8.9x10^{-4}$µs, which is larger than the WSSe@Se/H_2S1 and WSSe@S/H_2S1 arrangements. The SPDOS of WSSe@Ses arrangement is shown in Figure 5.7(i), which confirms the overlapping of H_2S and WSSe@Ses orbitals. The NH_3 molecule is also tested on WSSe@Ses monolayer. Figure 5.7(b) illustrates the optimized geometry of NH_3 adsorbed at WSSe@Ses monolayer and found the adsorption height around 2.94Å, confirming the vdW interaction. Bader charge analysis shows the 0.024e charge transfer from host to molecule. The optimized structure showed that $NH_3$is adsorbed from N site towards the WSSe@Ses. The adsorption energy and recovery time are – 0.20 eV and $2.8x10^{-3}$µs, respectively. The CDD plot shows the charge accumulation at the WSSe@Ses and charge depletion at H_2S. Figure 5.7(f) depicts the SPDOS of NH_3 adsorb on WSSe@Ses and found that the orbital contribution of NH_3 and WSSe@Ses are overlapping and symmetry in spin up and spin down state confirm the non-magnetic semiconducting nature. The optimized geometry of NO_2 adsorbed on WSSe@Ses is shown in Figure 5.7(c), which illustrates the 2.83 Å adsorption distance and confirms the vdW interaction between them. The Bader charge analysis also confirms the 0.12e charge transfer from host to adsorbate. The CDD plot endorses the charge accumulation at the adsorbate, validating the Bader charge analysis. The computed adsorption energy is - 0.28 eV, and recovery time is $4.7x10^{-2}$µs. The SPDOS ensures the spin splitting and additional states in VB and CB due to adsorption of NO_2, suggesting the magnetic behavior with $1\mu_B$ magnetic moment. Figure5.7(d) shows the optimized geometry of NO adsorbs on WSSe@Ses, and shows the 3.08Å adsorption height, substantiating the vdW interaction. The WSSe@Se monolayer transfer 0.01 e charge to NO molecule. The CDD plot ensures the charge accumulating at the NO molecule, which validates the Bader charge analysis. The calculated adsorption energy

is -0.15 eV. The SPDOS confirms the no additional electronic states occurred due to NO adsorption.

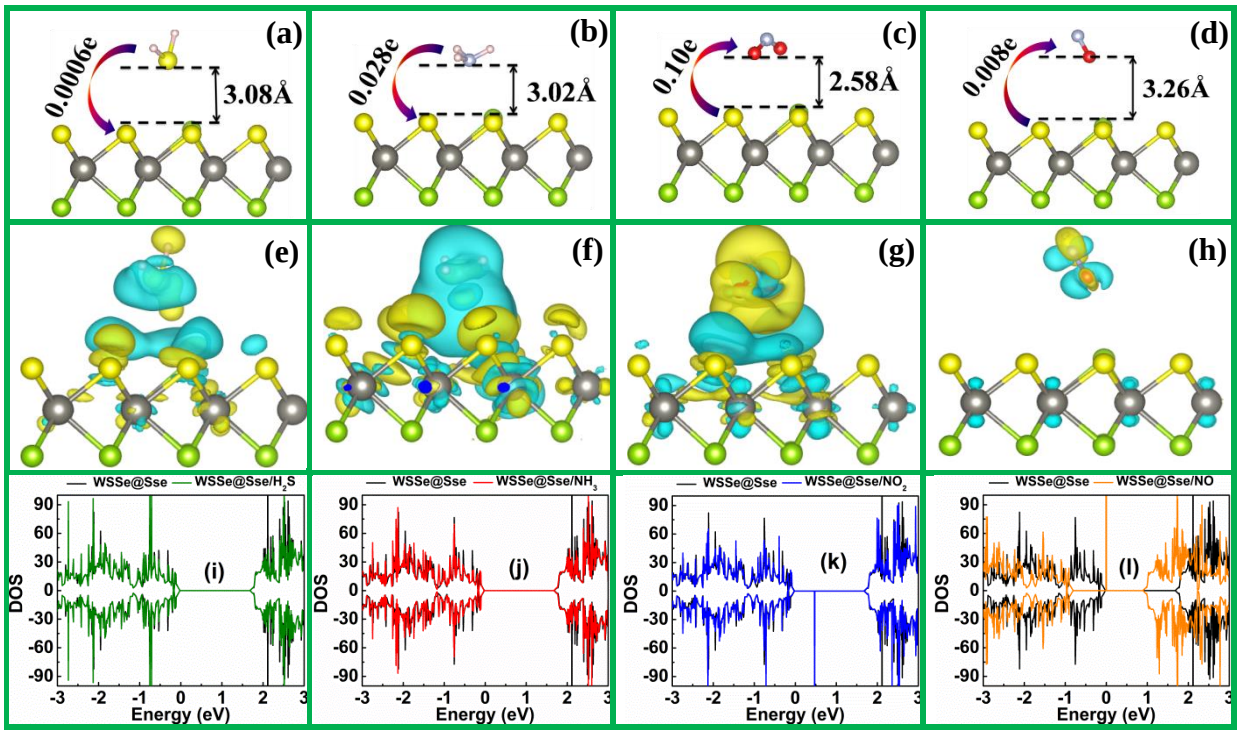

Figure 5.8 (a-d) Optimized geometries, (e-h) charge density difference and (i-l) SPDOS of gas molecules adsorb on WSSe@Sse monolayer. (Isosurface value 10^{-4} e/Å^3, the yellow color corresponds to charge accumulation, and blue color corresponds to charge depletion)

The WSSe@Sse monolayer is also tested for adsorption of the gases. The relaxed geometry of H_2S adsorbed on WSSe@Sse monolayer is depict in Figure 5.8(a) and found the adsorption height 3.08 Å, confirming the vdW interaction among them. The adsorption energy and recovery time for H_2S are –0.13 eV and 1.7x10^{-4}µs, respectively. Bader charge analysis confirms the 0.006e charge transfer from adsorbate to host, ensure the charge depletion nature of H_2S. Figure5.8(e) illustrates the charge depletion at the H_2S molecule and charge accumulating at the WSSe@Sse monolayer, which validates the Bader charge analysis. The SPDOS ensures the strong overlapping of H_2S and WSSe@Sse orbitals and symmetry in both the spin confirm the non-magnetic behavior. The adsorption of NH_3 molecule also examine on the WSSe@Sse monolayer. The relaxed structure shows the 3.02Å adsorption height and 0.028e charge from adsorbate to host. Bader charge analysis ensures the donor nature of NH_3 and adsorption height confirms the vdW interaction between NH_3 and WSSe@Sse. The adsorption energy is –0.20 eV, and recovery time is 2.1x10^{-3} µs for NH_3 molecule adsorb on WSS@Sse. Figure 5.8(j) illustrates the SPDOS and no additional energy states are observed in the forbidden region, and symmetry in both the spin ensures the non-magnetic semiconductor nature. The WSSe@Sse arrangements are more sensitive for the NH_3 molecule over the H_2S molecule. The relaxed geometry of NO_2 molecule adsorbed on WSSe@Sse is shown in Figure 5.8(c). The adsorption height found around 2.58Å, which is smaller than NO_2 adsorbed on WSSe@Ses. Bader charge analysis shows the 0.10 e charge from WSSe@Sse to NO_2 molecule, confirming the acceptor nature of NO_2 molecule. The adsorption energy and recovery time are –0.23eV and 8.7x10^{-3}µs, respectively. The CDD plots show the charge accumulation at the NO_2 molecule and validate the Bader charge analysis. The SPDOS ensures the defect states in the forbidden region due to NO_2 adsorption and asymmetry in spin states induce the ~ 1μ_B magnetic moment. The relaxed geometry of NO adsorb on WSSe@Sse monolayer is shown in Figure 5.8(d). The adsorption distance is around 3.26Å, suggesting the vdW interaction between them. The CDD plot shows the charge accumulation at the NO and charge depletion at

WSSe@Sse. The Bader charge analysis shows the 0.008e charge transfer from WSSe@Sse to NO molecule, and validating the CDD. The calculated adsorption energy is -0.09eV and recovery time found around $3.2x10^{-5}$ µs. The SPDOS is shown in Figure 5.8(l), which ensure the defect states in the forbidden region and asymmetry in the spin states confirm the magnetic nature due to NO adsorption.

5.3.4 Electronic properties of vacancy defects including MoSSe monolayers

We have considered the selenium surface of MoSSe monolayer because it showed better gas sensing properties for WSSe monolayer, reported in the above section. Here, we considered two types of vacancy defects, selenium vacancy (V_{Se}) and sulfur/selenium vacancy ($V_{S/Se}$) in MoSSe monolayer. These vacancy defects are introduced by removing the atoms from the supercell. The formation energy is –3.16 eV and -3.12 eV/atom corresponding to the MoSSe@ V_{Se} and MoSSe@$V_{S/Se}$ monolayer, respectively. The detailed analysis of vacancy defects in MoSSe monolayer is discussed by Chaurasiya et al. (Chaurasiya & Dixit, 2019). The spin-polarized band structure of WSSe@V_{Se} monolayer shows the additional states below the conduction band and above of the valence band due to the unsaturated bonds of tungsten atom near to defects site. The bandgap observed around 1.54eV and 1.37eV for WSSe@V_{Se} and MoSSe@$V_{S/Se}$ monolayer, respectively. The VB and CB both are dominated by W-d orbitals, and defect states also have W-d orbital contribution, shown in Figure 5.9. The symmetry in spin up and down states ensures the non-magnetic semiconductor nature. Figure 5.9(b) shows the spin-polarized band structure with TDOS of WSSe@$V_{S/Se}$ monolayer. It has similar electronic behavior like the WSSe@V_{Se} monolayer. The band structure of WSSe@V_{Se} and WSSe@$V_{S/Se}$ monolayer confirm the defect states below the CB which acts as the n-type semiconductor behavior due to unsaturated bonds of tungsten atoms.

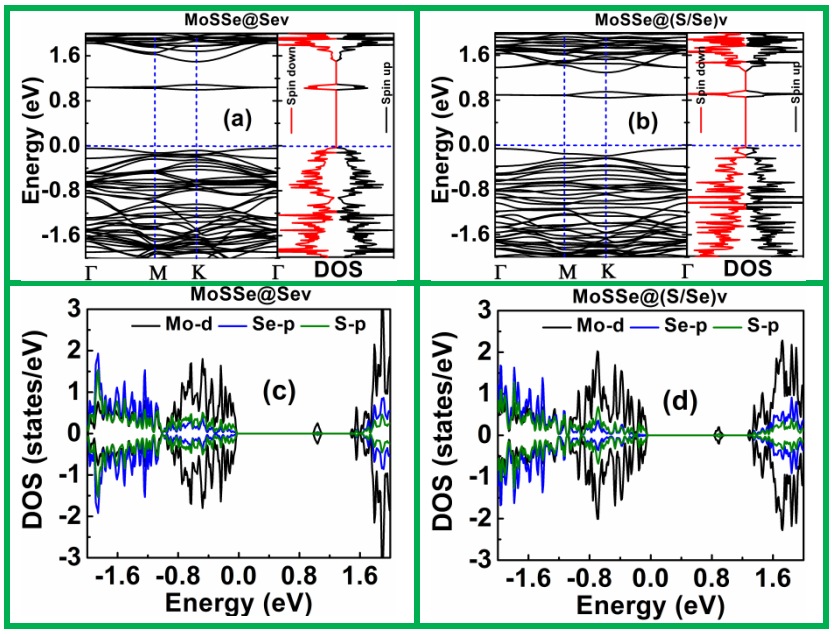

Figure 5.9 (a) and (b) are the band structure; (c) and (d) PDOS of MoSSe@Sev and MoSSe@$V_{S/Se}$ monolayer, respectively.

5.3.5 Adsorption of toxic gas molecules on pristine MoSSe monolayer

The optimized structure of H_2S molecule adsorbed on the host surface is shown along with the optimized structural parameters is reported in Figure 5.10(a&b). The interaction of H_2S with the H atom side on the host surface is renamed as P, and adsorption from the S site is renamed as P1. Bader charge analysis ensures 0.011e charge allocation from MoSSe to H_2S in P configuration; confirm the acceptor nature of H_2S. However, The P1 arrangement shows the

0.001e charge transfer from H_2S to MoSSe, Figure 5.10(b). The adsorption height among the host and adsorbate for P and P1 configurations is 2.292Å and 3.019Å, respectively. The relatively small adsorption height for P arrangement ensures that H_2S molecule has strong interaction because of the opposite nature of H atom and host surface. The P arrangement ensures the high adsorption energy, -0.156eV compare to the P1 arrangement adsorption energy, -0.147 eV. The computed adsorption energy is more than MoS_2 adsorption energy -0.120eV (Song & Lou, 2018) and lower than $MoSe_2$ adsorption energy -0.18eV (Natkaeo, Phokharatkul, Hodak, Wisitsoraat, & Hodak, 2018). Figure 12(a) shows the adsorption energy for P and P1 arrangements. Figure 5.10(a&b) shows the charge transfer among the adsorbate and host, and CDD validates the same results. The electronic properties of H_2S adsorbed monolayer are not showing any changes in the forbidden region of band structure compared to MoSSe monolayer, shown in figure 5.11(a). This confirms that the energy states of MoSSe and H_2S are overlapping. The symmetry in spin up and spin down states ensure the non-magnetic semiconductor properties of H_2S adsorb MoSSe.

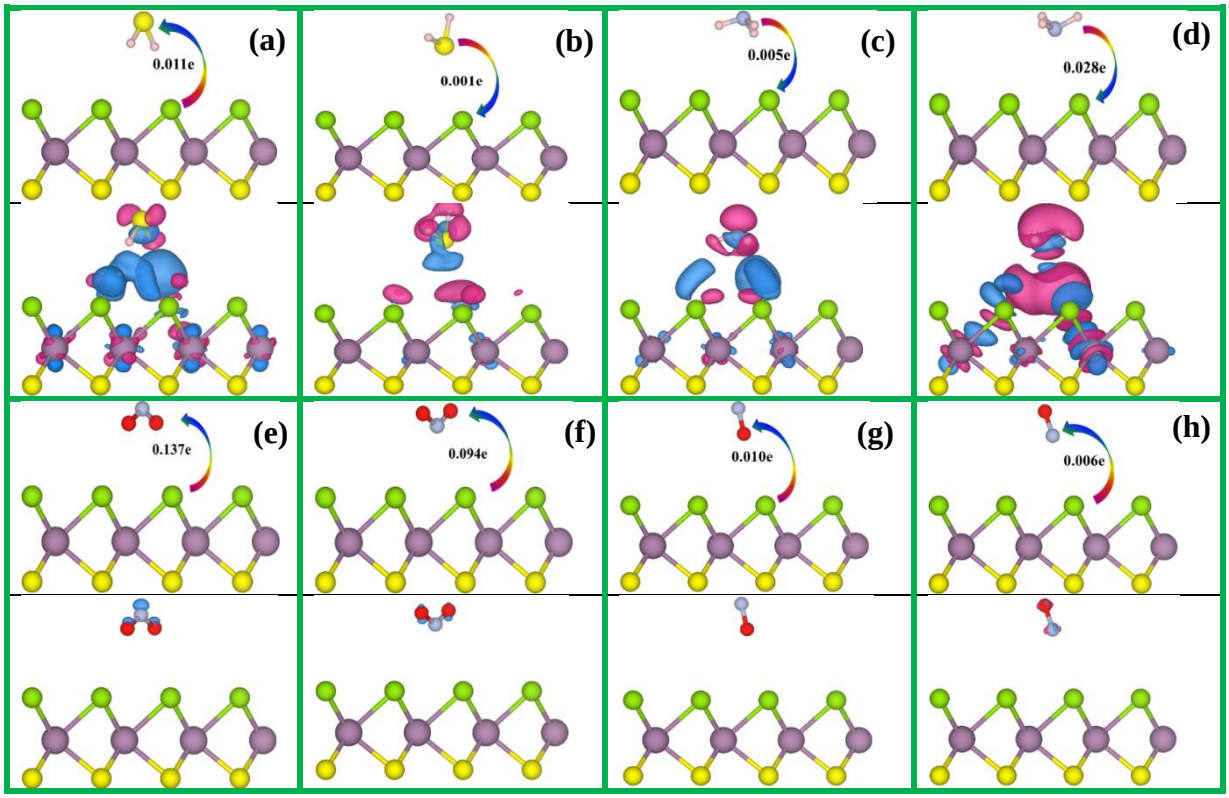

Figure 5.10 Optimized geometries and charge density difference of H_2S adsorb on MoSSe (a&b), NH_3 adsorb on MoSSe (c&d), NO_2 adsorb on MoSSe (e&f) and NO adsorb on MoSSe (g&h). (Pink, yellow, grey, green, dark blue and red represents the hydrogen, sulfur, nitrogen, selenium, molybdenum and oxygen, respectively)

NH_3 molecule adsorbs from the hydrogen site and nitrogen site on the MoSSe monolayer, shown Figure 5.10(c&d). When NH_3 molecule adsorbs from the hydrogen site on MoSSe layer is presented as P. Moreover, when NH_3 molecule adsorbs from the N site is represented as P1. NH_3 molecule transfer 0.005e charge to MoSSe in P arrangement. The P1 arrangement shows identical behavior and transfers 0.028e charge from NH_3 to MoSSe. NH_3 molecule is showing donor behavior because the Fermi level of MoSSe may lie between the HOMO and LUMO of NH_3 (C. Zhou, Yang, & Zhu, 2015). The obtained results are well-matched with the NH_3 adsorbed on MoS_2 and WS_2 monolayer, but the sensing behavior is better than previous reports (Yue, Shao, Chang, & Li, 2013; B. Zhao et al., 2016). Figure 5.12(a&b) shows the adsorption energy and adsorption height for P and P1 arrangements, which ensures the physisorption. The adsorption energy shows that P1 arrangement shows more sensitivity compared to P arrangement. NH_3 molecule showed the charge transfer to MoSSe monolayer; that's why the electrical conductivity should

improve. Similar results have been reported experimentally (Huo et al., 2014) in the case of NH_3 adsorption on WS_2 based FET. The spin-polarized band structure of MoSSe compared with NH_3 adsorbed MoSSe, shows the overlapping of NH_3 and MoSSe energy states; that's why no additional peaks are observed. The symmetry in the spin up and down states, confirms the non-magnetic semiconductor, shown in Figure 5.11(b). Figure 5.10(c&d) illustrates the CDD for P and P1 arrangement and validates the Bader charge, confirming the physisorption among them.

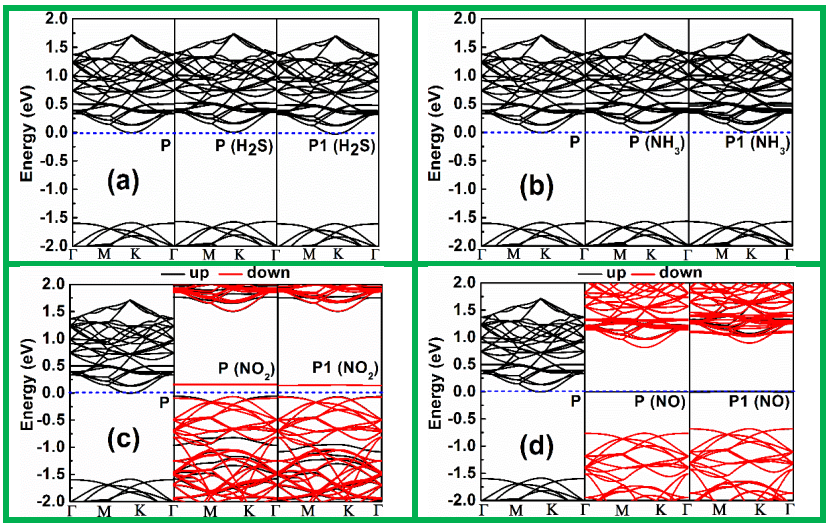

Figure 5.11 Comparison of band structure of pristine monolayer with the gas molecule adsorbed on MoSSe monolayer (a) H_2S, (b) NH_3, (c) NO_2 and (d) NO.

The optimized geometry of P and P1 arrangements are presented in Figure 5.10(e&f) and showing the 0.137e and 0.094e charge transfer from host to the molecule, ensuring the acceptor nature of NO_2 and validating the CDD. The reason may be LUMO of NO_2 lies below the Fermi level of MoSSe (C. Zhou et al., 2015). The identical results are investigated in MoS_2 and WS_2 monolayer for NO_2 molecule (Cho et al., 2015; C. Zhou et al., 2015). The adsorption energy for P and P1 arrangements are - 0.252 eV and - 0.024 eV, respectively, and corresponding adsorption height is listed in Figure 5.12(a&b), supporting the physisorption between the adsorbate and host in both the arrangements. The bond length of NO_2 molecule is elongated by 0.01Å due to adsorption on host surface. The band structure of NO_2 adsorbed monolayer is compared with the pristine monolayer and found the localized states above the valence band due to the presence of NO_2 molecule, shown in Figure 5.11(c). The same nature has been observed (C. Zhou et al., 2015) for NO_2 molecule adsorbed on WS_2 monolayer. The asymmetry in the spin up and spin down states induced the $0.99\mu_B$ and $1.02\mu_B$ magnetic moment for P and P1, respectively. The obtained result is well matched NO_2 adsorption on MoS_2 monolayer (Sahoo, Wang, Zhang, Shimada, & Kitamura, 2016) The MoSSe monolayer shows the better sensing properties for NO_2 molecule compare to MoS_2 and WS_2 monolayers.

Figure 5.10 (g&h) shows the optimized geometries for P and P1 arrangements and shows the 0.010e and 0.006e charge transfer from host to molecule, ensuring the acceptor nature of NO. The charge transfers from host to molecule because LUMO of molecule lies below the Fermi level of host (C. Zhou et al., 2015). The adsorption energies are -0.089 eV and -0.117 eV for P and P1 arrangements, respectively, plotted in Figure 5.12(a). However, the adsorption heights are 2.748 Å and 2.624Å for P and P1 arrangements, respectively, shown in Figure 5.12(b). An identical result has been observed on MoS_2 monolayer for NO adsorption (Yue et al., 2013). Figure 5.11(d) shows the band structure for P and P1 arrangements and found the additional bands near to the Fermi level. The additional bands due to NO adsorption induce the spin splitting and showed $1\mu_B$ magnetic moment. An identical study has been reported for NO adsorption on MoS_2

monolayer (Hongxing Li, Huang, & Cao, 2016). Pristine MoSSe monolayer is n-type, but the charge transfers from host to molecule covert into p-type semiconductor (Hai Li et al., 2012). The charge depletion in monolayer due to NO adsorption, the conductivity will decrease.

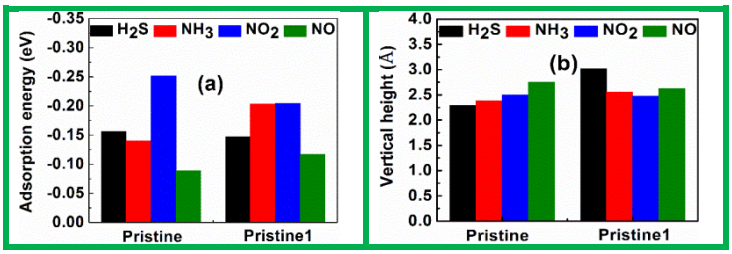

Figure 5.12 (a) Adsorption energy and (b) vertical height of gas molecules adsorb on pristine MoSSe monolayer

5.3.6 Adsorption of toxic gas molecules on vacancy defect including MoSSe monolayers

The defect included monolayers are also considered for gas adsorption. Here, we have considered the MoSSe@V_{Se} and MoSSe@$V_{S/Se}$ monolayer for the adsorption. The optimized configuration and Bader charge for H_2S adsorbed on MoSSe@V_{Se} and MoSSe@$V_{S/Se}$ monolayer are shown in Figure 5.13 (a&b) and Figure 5.14 (a&b), respectively. The maximum adsorption energy (adsorption distance) is -0.238eV (1.61Å), correspond to MoSSe@$V_{S/Se}$ monolayer, shown in Figure 5.17(a&b). The lower adsorption energy with higher adsorption height supports the physisorption between the H_2S adsorption and monolayers. We found the best configuration for H_2S molecule on MoSSe@V_{Se} and MoSSe@$V_{S/Se}$ monolayers in terms of the adsorption energy, adsorption height, and charge transfer. The MoSSe@V_{Se} and MoSSe@$V_{S/Se}$ monolayers transfer 0.017e and 0.018e charge to H_2S. Due to the acceptor behavior of the H_2S, the resistance of channel will increase, and the unsaturated bonds of the Mo atoms repel the positive charge of H atom; that's why the H-S bond length has improved by 0.002Å. However, the sulfur site of H_2S molecule, attract towards the defect included monolayer. The adsorption heights confirm the vdW interactions between the adsorbate and host. The band structure of H_2S adsorbed on MoSSe@V_{Se} and MoSSe@$V_{S/Se}$ monolayers showed strong overlapping and no additional states are observed, shown in Figure 5.15(a) and 5.16(a), respectively. The above studied adsorption of H_2S, confirms that MoSSe@$V_{S/Se}$ monolayer showed the strong adsorption.

The NH_3 adsorption behavior also examined on MoSSe@V_e and MoSSe@$V_{S/Se}$ monolayers. The optimized geometry and CDD of NH_3 adsorb MoSSe@V_{Se} and MoSSe@$V_{S/Se}$ monolayer along with the charge transfer is shown in Figure 5.13(c&d) and Figure 5.14(c&d), respectively. The adsorption height confirms the physisorption between the NH_3 molecule and defect monolayers. Bader charge analysis predicts the 0.019e and 0.001e charge from MoSSe@V_{Se} monolayer to NH_3 molecule and validates the CDD. The computed adsorption energies are -0.281eV and -0.216eV for MoSSe@V_{Se}/NH_3 and MoSSe@$V_{S/Se}$/$NH_3$1 arrangements, respectively, shown in Figure 5.17(a). The MoSSe@V_{Se} monolayer showed improvement in the sensitivity of NH_3 molecule compare to P and P1 arrangements. Since the charge transfer from host to adsorbate so the electrical conductivity may decrease. The sensible adsorption energy may exhibit a good recovery time. The MoSSe@$V_{S/Se}$ monolayer is evaluated as the host for adsorption of NH_3 molecule. The Bader charge analysis shows the 0.022e and 0.003e charge transfer from molecule to monolayer for MoSSe@$V_{S/Se}$/NH_3 and MoSSe@$V_{S/Se}$/$NH_3$1 arrangements, respectively. That's why the electronic conductivity may increase due to NH_3 adsorption. The adsorption energies are - 0.274 eV and - 0.177 eV for MoSSe@$V_{S/Se}$/NH_3 and MoSSe@$V_{S/Se}$/$NH_3$1 arrangements, respectively, shown in Figure 5.17(a). The band structure doesn't show any additional peak due to the adsorption of NH_3 molecule, and symmetry in spin up and spin down states confirm the non-magnetic semiconducting behavior, shown in Figure 5.15(b) and Figure 5.16(b). The above studies suggest that defects improve the sensitivity of NH_3 molecule with a fast recovery time.

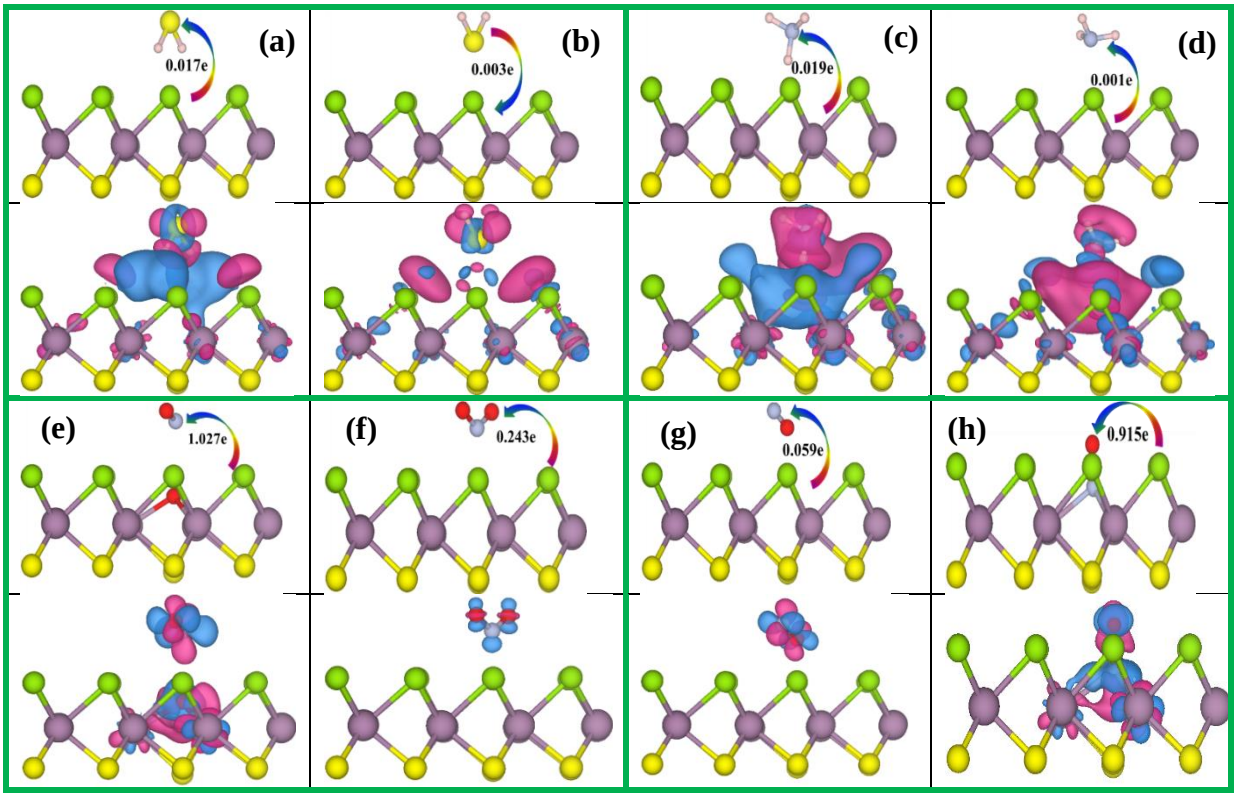

Figure 5.13 Optimized geometries and charge density difference of H_2S (a&b), NH_3 (c&d), NO_2 (e&f) and NO (g&h) adsorb on MoSSe@V_{Se} monolayer. (Pink, yellow, grey, green, dark blue and red represents the hydrogen, sulfur, nitrogen, selenium, molybdenum and oxygen, respectively)

Figure 5.13(e&f) shows the relaxed geometries of NO_2 adsorbed on MoSSe@V_{Se} monolayer. The MoSSe@V_{Se} /NO_2 arrangements show that NO_2 molecule dissociates and act as oxygen doped in host with NO adsorption. The bond length of NO is around 1.61Å, which is equal to NO molecule. The adsorption energy for MoSSe@V_{Se} /NO_2 arrangement is -3.36 eV and 1.027e charge transfer is noticed from host to adsorbate, confirming the acceptor behavior of NO molecule. An identical study has been carried out on the selenium defect included WSe_2 monolayer for NO_2 adsorption (D. Ma et al., 2017). Figure 5.15(c) shows the band structure of MoSSe@V_{Se}/NO_2 and MoSSe@V_{Se}/$NO_2$1 arrangement and compared it with MoSSe@V_{Se} monolayer. It is observed that selenium defects may overcome due to oxygen doping. The band structure shows the spin splitting in spin up and spin down states, suggesting the onset of 1μ_B magnetic moment, shown in Figure 5.15(c). Figure 5.13(f) shows the relaxed geometry of MoSSe@V_{Se}/$NO_2$1 arrangements and showing the 0.243e charge transfer from host to molecule. The CDD plot validates the Bader charge analysis. The adsorption energy and adsorption height of MoSSe@V_{Se} /$NO_2$1 arrangement are -0.288eV and 1.518Å, respectively, shown in Figure 5.17.A large value of adsorption energy ensures the long recovery time. The optimized geometry of MoSSe@$V_{S/Se}$/NO_2 arrangement is shown in Figure 5.14(e). The MoSSe@$V_{S/Se}$ /NO_2 arrangements show a similar behavior to MoSSe@V_{Se}/NO_2 arrangements. The NO_2 molecule dissociates and oxygen atom forming the covalent bond with the nearby molybdenum atoms. The adsorption energy for MoSSe@$V_{S/Se}$/NO_2 arrangement is -3.404eV, which suggests a very high recovery time. Figure 5.16(c) shows the band structure for MoSSe@$V_{S/Se}$/NO_2 arrangements and confirm the spin splitting among the spin up and spin down states, showing 1.10μ_B magnetic moment. Bader charge analysis shows the 1.077e charge transfer from host to molecule. The adsorption energy for MoSSe@$V_{S/Se}$/$NO_2$1 arrangement is -0.273 eV smaller than MoSSe@$V_{S/Se}$/NO_2 arrangement, and adsorption height is 1.534Å. In case of MoSSe@$V_{S/Se}$/$NO_2$1 arrangement, the NO_2 molecule accepts 0.257e charge from the host and ensures the acceptor nature. The Bader charge analysis validates the CDD.

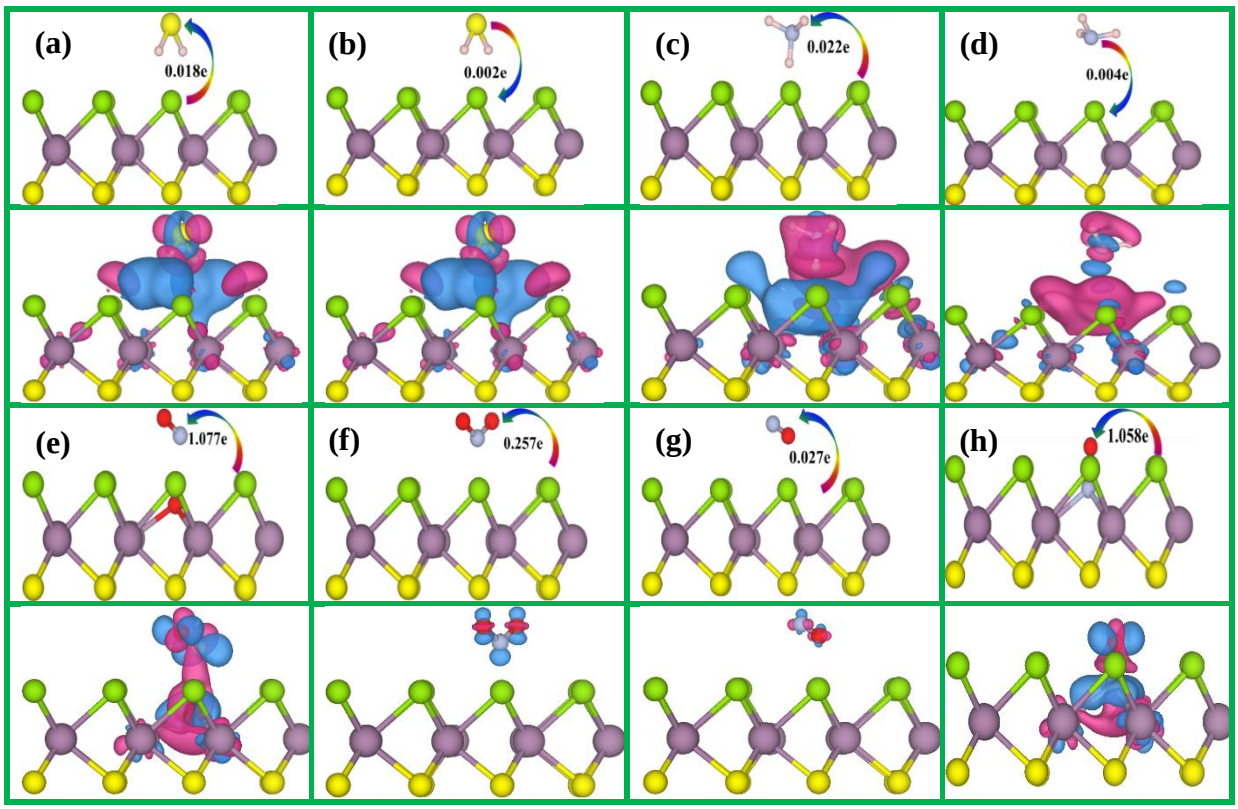

Figure 5.14 Optimized geometries and charge density difference of H_2S (a&b), NH_3 (c&d), NO_2 (e&f) and NO (g&h) adsorb on MoSSe@$V_{S/Se}$ monolayer. (Pink, yellow, grey, green, dark blue and red represents the hydrogen, sulfur, nitrogen, selenium, molybdenum, and oxygen, respectively)

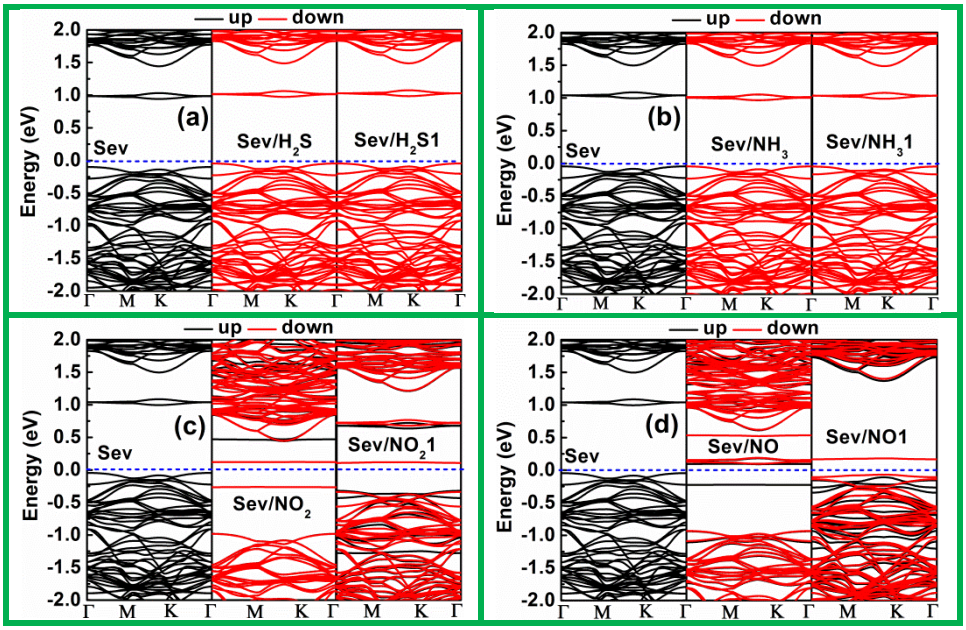

Figure 5.15 Comparison of band structure of pristine monolayer with the gas molecule adsorbs on MoSSe@ V_{Se} monolayer (a) H_2S, (b) NH_3, (c) NO_2 and (d) NO.

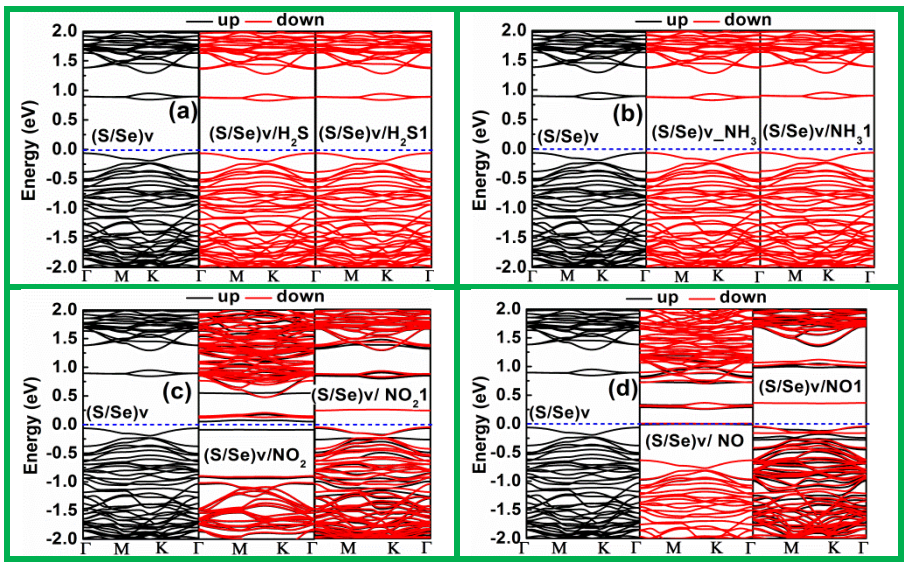

Figure 5.16 Comparison of band structure of pristine monolayer with the gas molecule adsorbs on MoSSe@ $V_{S/Se}$ monolayer (a) H_2S, (b) NH_3, (c) NO_2 and (d) NO.

The adsorption of NO molecule on the MoSSe@V_{Se} is also studied, and optimized structures are shown in Figure 5.13(g&h). Bader charge analysis shows the 0.059e and 0.915e charge from host to molecule for MoSSe@V_{Se}/NO and MoSSe@V_{Se}/NO1 arrangements, respectively, confirming the acceptor nature. The large charge transfer in MoSSe@V_{Se}/NO1 arrangements is due to the formation of covalent bonding with the neighbor molybdenum atoms. The covalent bond formation ensures the chemisorption, and thus, the recovery time will be relatively large. The CDD plot validates the chemisorption. Figure 5.15(d) depicts the band structure for MoSSe@V_{Se} /NO and MoSSe@V_{Se}/NO1 arrangements and found the defect states in the VB and CBs. Moreover, the spin splitting induces the 1.07 and 1.12 μ_B magnetic moment due to NO adsorption. MoSSe@$V_{S/Se}$ defect also considered as a host for NO adsorption. The relaxed MoSSe@$V_{S/Se}$/NO and MoSSe@$V_{S/Se}$/NO1 geometries are shown in Figure 5.14 (g&h). The MoSSe@$V_{S/Se}$/NO arrangement ensures the 0.027e charge host to molecule and adsorption height confirm the physisorption. Moreover, the MoSSe@$V_{S/Se}$/NO1 arrangements transfer 1.058e charge from host to molecule. The computed adsorption energies for MoSSe@$V_{S/Se}$/NO and MoSSe@$V_{S/Se}$/NO1 arrangements are -0.083 eV and -2.894 eV, respectively, shown in Figure 5.17(a). The very high adsorption energy and large charge transfer in MoSSe@$V_{S/Se}$ /NO1 arrangements showed the chemisorption. Due to the formation of a chemical bond with NO in MoSSe@$V_{S/Se}$/NO1 arrangements, the bond length of NO is elongated by 0.13Å. The CDD validates the Bader charge analysis and confirms the chemisorption in MoSSe@$V_{S/Se}$ /NO1 arrangements. Figure 5.16(d) shows the band structure with spin splitting induce the magnetic of 1.0μ_B.

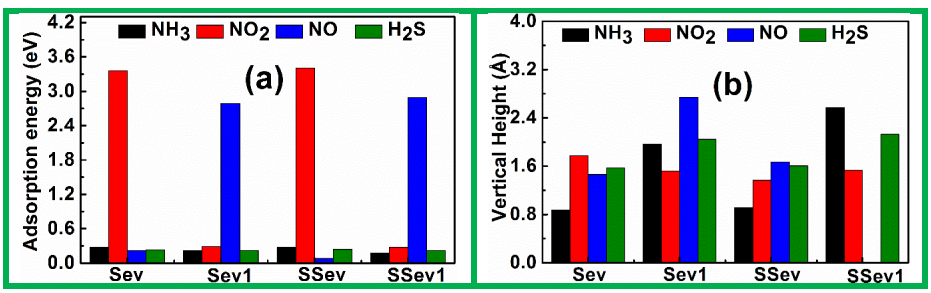

Figure 5.17 (a) Adsorption energy and (b) vertical height of gas molecules adsorb on MoSSe@Sev and MoSSe@$V_{S/Se}$ monolayer.

5.4 Conclusion

In this chapter, we have studied the electronic properties of vacancy and antisite defects in monolayers. The antisite defects are more stable over the vacancy defects. The adsorption of gases, H_2S, NH_3, NO_2, and NO are investigated on pristine MoSSe and WSSe monolayers with different chalcogen surfaces and diverse orientations of gas molecules. Adsorption on pristine WSSe monolayer ensures the high sensitivity for selenium surfaces. NO_2 molecule has high adsorption energy for MoSSe and WSSe monolayers. The order of sensitivity is NO_2>NH_3>H_2S>NO. The recovery time confirms the fast recovery for gas molecules. WSSe monolayer showed the higher sensitivity compared to MoSSe monolayer. The antisite and vacancy defects improved the gas sensing properties compared to antisite defects.